

## 26. PHYSICAL PROPERTIES OF REPRESSURIZED SEDIMENT FROM HYDRATE RIDGE<sup>1</sup>

William J. Winters,<sup>2</sup> William F. Waite,<sup>2</sup> David H. Mason,<sup>2</sup>  
and Lauren Y. Gilbert<sup>2</sup>

### ABSTRACT

As part of an ongoing laboratory study, preliminary acoustic, triaxial strength, and electrical resistivity results are presented from a test performed on a clayey silt sediment sample recovered from Site 1249 at the summit of southern Hydrate Ridge during Ocean Drilling Program Leg 204. The test specimen was stored and transported in two different methane-charged pressure vessels until it was tested using the Gas Hydrate and Sediment Test Laboratory Instrument (GHASTLI). Although gas hydrate may have existed in the core section immediately after recovery, little (if any) hydrate was present in the specimen during testing. We therefore present background physical property results for sediment that may have hosted gas hydrate in situ. Because we consolidated the test specimen in increments beyond its in situ stress state, we are able to present properties representative of similar but deeper sub-bottom sediment. The increased consolidation stress also helped to mitigate some, but not all, types of disturbance caused by the recovery process. *P*-wave velocities from 1.54 to 1.74 km/s varied linearly with consolidation stress,  $\sigma'_c$ , up to 970 kPa (equivalent to ~160 meters below seafloor). Electrical resistivity was periodically measured by a Wenner array and varied between 1.0 and 2.8  $\Omega$ m. These values reflect both the pore water salinity and soft, fine-grained texture of the sediment. Shear behavior is consistent with the induced normally consolidated behavior of clayey silt.

<sup>1</sup>Winters, W.J., Waite, W.F., Mason, D.H., and Gilbert, L.Y., 2006. Physical properties of repressurized sediment from Hydrate Ridge. In Tréhu, A.M., Bohrmann, G., Torres, M.E., and Colwell, F.S. (Eds.), *Proc. ODP, Sci. Results*, 204, 1–19 [Online]. Available from World Wide Web: <[http://www-odp.tamu.edu/publications/204\\_SR/VOLUME/CHAPTERS/119.PDF](http://www-odp.tamu.edu/publications/204_SR/VOLUME/CHAPTERS/119.PDF)>. [Cited YYYY-MM-DD]

<sup>2</sup>U.S. Geological Survey, 384 Woods Hole Road, Woods Hole MA 02543, USA. Correspondence author: [bwinters@usgs.gov](mailto:bwinters@usgs.gov)

Initial receipt: 17 April 2005

Acceptance: 17 April 2006

Web publication: 3 October 2006

Ms 204SR-119

## INTRODUCTION

We determined acoustic, shear strength, and electrical resistivity properties of a natural clayey silt specimen recovered from the summit of southern Hydrate Ridge during Leg 204. Little, if any, gas hydrate existed in the sediment during testing; however, the measurements provide important baseline information on the properties of host sediment that may contain hydrate in situ. Although hydrate occurs in a wide variety of sediment types and is abundant at some locations, data are sparse about how it forms, behaves, and interacts with sediment.

The sample was obtained in 778 m of water from interval 204-1249I-4H-3, 40–120 cm, at a subbottom depth of 26.23–26.83 meters below seafloor (mbsf) (44°34.2111'N, 125°8.8437'W). With logistical cooperation from the Ocean Drilling Program (ODP), the sample was stored within two different methane-pressurized vessels and transported overland to College Station, Texas (USA), and subsequently moved by airfreight to its final destination in Woods Hole, Massachusetts (USA). There, it was tested using the Gas Hydrate and Sediment Test Laboratory Instrument (GHASTLI).

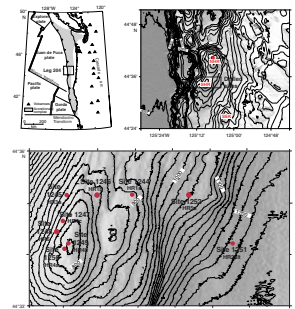
A reduced number of physical property measurements were conducted at Site 1249 because of sample disturbance issues. The sample tested in GHASTLI was therefore consolidated incrementally beyond its in situ stress state to mitigate some, but not all, types of sample disturbance (Ladd and Foott, 1974) and obtain property estimates representative of similar but deeper sediment. Results presented here are from the first of a two-part study. During the second part of the study, we plan to form methane gas hydrate within a similar, adjacent sediment sample to determine the effect of hydrate on fine-grained sediment properties and behavior. Knowledge of that behavior is fundamental to remotely quantifying in situ gas hydrate and assessing economic and geohazard potential.

## GEOLOGIC SETTING

During Leg 204, a total of nine sites on the Oregon continental margin were logged and subsequently cored (Fig. F1) in water depths from 778 to 1218 m. The objectives of the cruise included determining the location and distribution of natural gas hydrate, mechanisms for gas and fluid flux into the gas hydrate stability zone, and interrelationships between hydrate and host sediment physical properties (Shipboard Scientific Party, 2003). Hydrate Ridge is a complex, tectonically active accretionary system formed by the Juan de Fuca plate subducting beneath North America. A widespread bottom-simulating reflector (BSR) exists in this region that suggests gas hydrate may be widespread throughout the area. In fact, hydrate has been observed and recovered during numerous expeditions to Hydrate Ridge (Bohrmann et al., 1998; Suess et al., 1999; Tréhu et al., 1999).

Site 1249, located on the summit of southern Hydrate Ridge, is a complicated region containing massive amounts of gas hydrate near the seafloor and gas bubble plumes in the water column at various locations. The BSR is estimated to occur at 115 mbsf (Shipboard Scientific Party, 2003). Twelve holes were drilled (to a maximum subbottom depth of 90 mbsf) and ten were cored at Site 1249. Approximately 224 m of hydrate-bearing sediment was cored from the summit with a 35% recovery rate. Overall recovery was 48%. Centimeter-scale layers of gas

F1. Site location map, Leg 204, p. 10.



hydrate interbedded with soft sediment (Shipboard Scientific Party, 2003) as well as massive chunks, nodules, and thin plates of hydrate were recovered (Tréhu et al., 2004).

## PROCEDURES AND EQUIPMENT

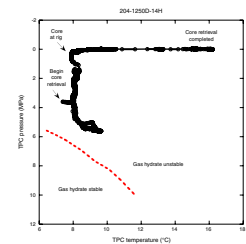
### Sample Storage, Transportation, and Setup

Natural gas hydrate is susceptible to dissociation when pressure decreases and temperature increases, as commonly occurs during drilling and coring recovery operations. This problem may actually be magnified by the very act of coring as exemplified by the pressure-temperature (P-T) plot of a core recovered from nearby Site 1250 (Fig. F2) (Ussler et al., this volume; Tréhu, this volume). Gas hydrate at this sub-bottom depth is stable; however, the act of coring brought the sample out of the hydrate stability field even before the core began its ascent. This highlights the need for pressure coring systems that maintain P-T conditions throughout the recovery process. After recovery, testing at in situ conditions without depressurizing the sample is optimal (C. Santamarina, pers. comm., 2006).

In addition to using pressure coring systems that retain in situ pressure during the entire retrieval process, conventionally recovered samples containing gas hydrate were placed in either liquid nitrogen or, in the case of the sample described here, stored in metal pressure vessels. The core was out of the gas hydrate stability field during initial recovery, during the examination and cutting process on deck, and during the transfer process into a 1-m-long pressure vessel. After the vessel was sealed, it was quickly pressurized to between 4.1 and 4.5 MPa with methane and stored at  $\sim 4^{\circ}\text{C}$ . The cores were kept in a refrigerated van during the overland trip to College Station, Texas, where they were stored in a specially designed Hazmat facility. Partly based on the results of gamma ray density logging (P. Schultheiss, pers. comm., 2003), a 1-m core section was depressurized in December 2003 at College Station and a 20-cm core section was subsampled. The subsample was repressurized to  $\sim 4.4$  MPa within a U.S. Department of Transportation (DOT)-exempted storage and transportation vessel. Gas hydrate was not observed on or within the core during the subsampling procedure (J. Firth, pers. comm., 2004). The stainless steel sample vessel was placed into a cooler filled with ice and secured using a custom-made plastic holder. This is the first time this DOT-exempted type of vessel was used to airfreight a sample containing gas hydrate to a U.S. destination (Woods Hole, Massachusetts) (Fig. F3).

Before the test sample was once more depressurized to atmosphere in Woods Hole, Massachusetts, an aliquot of gas was collected and stored in a previously evacuated 75-mL stainless steel vessel. The pressure was slowly (4 min total) bled off to prevent icing of the fill-valve internal components. The sample (Fig. F4) was removed from the pressure vessel and prepared within a top-loading freezer to minimize further gas hydrate dissociation caused by exposure to warm room temperatures. Prior to extrusion, a small white patch on the surface of the sample quickly disappeared without exhibiting the typical bubbling nature of dissociating gas hydrate. The patch may have been ice caused by endothermic cooling during depressurization. To reduce sample disturbance, a thin stainless steel wire was used to break the adhesion between the soft sediment and the core liner prior to extrusion from the liner. Sam-

F2. Pressure vs. temperature path, p. 11.



F3. DOT-exempted pressure vessel, p. 12.



F4. Test sample after extrusion, p. 13.



ple preparation was problematic. The friable nature of the very soft, clayey silt made it difficult to trim the sample and obtain smooth, parallel ends. Furthermore, some surface voids in the sample required filling with sediment left over from the trimming process. Subsamples were removed for moisture and density (MAD) measurements, including water content, grain size, and grain density. One sample was stored in liquid nitrogen for planned scanning electron microscope (SEM) characterization. The remaining part of the specimen was jacketed for testing in GHASTLI, and the mass, length, and diameter of the test specimen were recorded.

## Laboratory Testing

### Moisture and Density

Physical property MAD measurements include water content, grain density, and grain size. Other parameters, such as wet bulk density, unit weight, void ratio, and porosity, were calculated from the water content and grain density values using two methods. The first method used the measured volume of the test specimen determined with calipers, and the second method assumed 100% of the pore space was saturated with water.

Water contents (related to mass of solid grains and total sample mass) were determined for the test specimen and trimmings dried at 105°C for at least 24 hr. All physical property calculations were corrected for the presence of residual salt left on the solid particles after oven drying, assuming a pore water salinity of 37 ppt based on shipboard measurements. In the natural environment, salt and other particles are dissolved in the pore fluid and behave as part of the aqueous phase. The calculations remove the salt precipitate from the solids and add it back to the fluid. The dried specimen was then ground into a powder or broken into granule-size pieces, and the volume of dried solids was determined with an automatic gas pycnometer using helium as the purge and expansion gas (ASTM International, 1997). The grain density of the pycnometer specimen was calculated using the mass of solids, as determined immediately prior to insertion of the sample into the pycnometer. All mass determinations were made quickly to reduce moisture in the air from being adsorbed by clay minerals that could have been present.

Grain sizes were determined using two methods. Dry sieving was used to measure the size of coarse material (>0.062 mm, silt/sand boundary) and a Coulter Counter particle size analyzer using the program CLAYEST to extrapolate data into a finer grain size range was used for the fine fraction (<0.062 mm).

### Gas Hydrate and Test Laboratory Instrument

GHASTLI utilizes a number of separate pressure and temperature control subsystems to simulate in situ conditions typically on a 71-mm-diameter by 130- to 140-mm-high right cylindrical sediment specimen (Fig. F5) (Winters et al., 2000). The specimen tested in this study averaged 60 mm in diameter and 134 mm in length. The trimmed specimen was placed between test end caps and was surrounded by three pressure-tight flexible membranes. The end caps incorporate acoustic transducers and gas or water flow ports. Sensor measurements from within the different subsystems and in close proximity to the test specimen are

F5. Test specimen about to be raised into the main pressure vessel, p. 14.



logged and displayed by a computer employing custom-designed Lab-view software. During testing, the sample resides within a pressure vessel filled with silicone oil. The flexible membranes applied to the sample within the top-loading freezer isolated the external silicone oil from the test sample after it was placed in the test chamber. Internal pore pressure and exterior chamber pressure were simultaneously raised to 12 MPa. Then the specimen was incrementally consolidated to 0.97 MPa by keeping the internal pressure constant and increasing the external chamber pressure.

Four separately controllable 500-mL syringe pumps are used to maintain the confining pressure surrounding the specimen and internal specimen pressures. Syringe pump flow rates range from 0.001 to >80 mL/min. The backpressure system contains a collector capable of separating and measuring water and gas volumes pushed out of the specimen at test pressures by gas hydrate dissociation (Winters et al., 2000). A separate fifth syringe pump controls the movement of the load ram during shear tests. The ram position determines the height of the specimen. Four thermocouples and four thermistors are placed against the outside perimeter of the specimen or end caps at different heights to measure temperature variations along the sample surface.

*P*-wave velocity ( $V_p$ ) is measured by pulse transmission along the length of the cylindrical sample using 500-kHz to 1-MHz (natural frequency) wafer-shaped crystals located on the back side (away from the specimen) of each end cap. A 400-V pulse is sent to the transmitting transducer and the received signal is amplified, digitized, displayed on a digital oscilloscope, and recorded by a computer.  $V_p$  is calculated from the specimen length/measured acoustic traveltime through the specimen.

Electrical resistivity was determined using an Advanced Geosciences, Inc., Sting R1 IP Earth resistivity meter. Flat electrodes (6 mm in diameter) were placed 27 mm apart in a Wenner array vertically oriented on the side of the test specimen. Current was automatically optimized to the external electrodes, and potential was measured by the internal electrodes.

Four parameters are measured during triaxial strength tests (Holtz and Kovacs, 1981): load, axial deformation, confining pressure, and pore pressure. Load is produced by a syringe pump-controlled ram contacting the heat exchanger, which then pushes on the sample. Movement of the ram, which can vary from 0.0001 to 2 mm/min, is measured using a linear displacement transducer connected to the load ram. For this test, a strain rate of 0.0019%/min was used, which required 145 hr to complete the shear phase, imparting 16.5% overall strain.

## RESULTS AND DISCUSSION

### Moisture and Density

Water content varied from 64.6% to 69.0% (relative to dry solid mass) and 39.2% to 40.8% (relative to total wet mass) and decreased to 54.2% and 35.2%, respectively, after the specimen was consolidated to 970 kPa (Table T1). Measured grain density of 2.67 g/cm<sup>3</sup> is consistent with MAD shipboard values (2.56–2.76 g/cm<sup>3</sup>; average = 2.7 g/cm<sup>3</sup>) from nearby Holes 1249B, 1249C, and 1249F at similar subbottom depths. Initial bulk density of the test sample and trimmings varied from 1.58 to 1.64

g/cm<sup>3</sup>, and porosity ranged from 62.7% to 64.2%. Shipboard porosities varied from 65.1% to 68.5%. This may indicate that the test sample became slightly denser during storage. Porosity varies greatly in the shipboard cores, however, so this observation is tentative.

The postconsolidation test specimen had a bulk density of 1.71 g/cm<sup>3</sup>. As expected, this is denser than the range of shipboard bulk densities. Those values ranged from ~1.55 g/cm<sup>3</sup> at the seafloor to 1.65 g/cm<sup>3</sup> at ~90 mbsf. The final consolidation stress imparted to the test specimen replicates a subbottom depth of ~160 m.

### Acoustic Properties

Determining the effect of increasing overburden on acoustic velocity is difficult with naturally occurring sedimentary deposits because of stratigraphic variability. Such is certainly the case for the Hydrate Ridge region. However, GHASTLI provides an opportunity for not only reducing the effects of sample disturbance, but determining pure overburden (consolidation) and velocity relationships as well.

Initial  $V_p$ , measured axially through the test specimen, is 1.54 km/s (Fig. F6), which is expected because of the very soft consistency of the sediment.  $V_p$  was also calculated for six additional consolidation increments between 35 and 970 kPa. Maximum  $V_p$  was 1.74 km/s. A very well defined linear correlation exists between  $V_p$  and consolidation stress. This relation is useful for modeling behavior of typical clayey silt present in the Hydrate Ridge area.

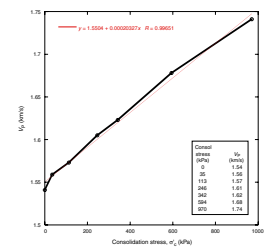
$V_p$  is highly variable in well logs obtained from adjacent Hole 1250F possibly reflecting the complex nature of this region, both geologically/tectonically and with respect to hydrate distribution and abundance. Velocity typically varies from 1.5 to 1.55 km/s over much of the interval from 76 to 164 mbsf. At 109 mbsf,  $V_p$  increased to 1.675 km/s.

### Electrical Resistivity Properties

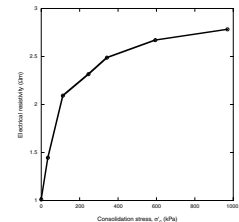
Electrical resistivity is a useful indicator of hydrate content because it increases significantly with hydrate pore saturation (Makogon, 1997). Electrical resistivities determined from a Wenner array varied from ~1.0 to 2.8  $\Omega$ m and increased with consolidation stress (Fig. F7). Electrical resistivity values are greater than that of seawater (Sharma, 1997) because of the presence of sediment grains. Electrical resistivity of water with a salinity of 37 ppt is ~0.25  $\Omega$ m at 10°C. Results are slightly low for clayey sediments, which theoretically have resistivity values ranging from 3 to 15  $\Omega$ m (Hunt, 1984), but this may be related to test pore water that is more saline than reported samples.

An understanding of our results can be formulated through a comparison with logging measurements from a nearby hole. In Hole 1249J, well-logging resistivity varies from ~0.5  $\Omega$ m near the seafloor to as much as 200  $\Omega$ m in layers containing significant amounts of gas hydrate. This range reflects the geologic complexity of the site as well as the influence of gas hydrate on electrical resistivity measurements. Interestingly, for 20 m near the bottom of the hole (68–88 mbsf), values are nearly identical (2–3  $\Omega$ m) to those measured in GHASTLI at the higher consolidation stresses. The increase in resistivity with consolidation stress may simply be related to the reduction in sediment water content and porosity during our GHASTLI test. Although well-logging

F6. P-wave velocity vs. consolidation stress, p. 15.



F7. Electrical resistivity vs. consolidation stress, p. 16.



measurements do not seem to reflect this same trend, it may be that lithologic changes mask this more subtle effect.

### Shear Strength Properties

Triaxial shear strength tests are performed because they simulate in situ states of stress and because resultant parameters, used to model sediment behavior, are difficult to obtain by other means. An undrained triaxial shear test was performed at a consolidation stress of 970 kPa. As shown in Table T1, the specimen volumetrically decreased by at least 38.8 cm<sup>3</sup> because of consolidation. Resultant water content (related to solids) decreased from 65.2% to 54.2% and porosity decreased from 62.9% (calculated) to 58.5%. This is expected given the very soft nature of the initial test specimen.

Interesting trends are apparent from the tabulated triaxial test data (Table T2) and the engineering plots (Fig. F8). Although the sample may have been initially disturbed because of sampling and possible gas hydrate dissociation, after consolidation the specimen behaved as a “normally consolidated” sample representative of in situ conditions.

This is exemplified by the following results, which are within the range for normally consolidated fine-grained sediment:

1. The pore pressure coefficient “A” = 1.12 (Bowles, 1979);
2. The strength to consolidation stress ratio,  $q_{max}/\sigma'_c = 0.31$  (Bowles, 1979); and
3. The effective friction angle = 29° (Lambe and Whitman, 1969).

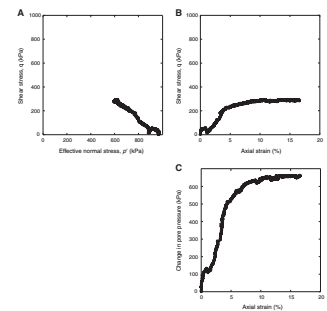
Because pore pressures greatly influence local effective stresses, knowledge of their magnitude is crucial when modeling the potential for slope instability and other geohazards. The triaxial strength test shows that pore pressure change always remains positive during shear (Fig. F8C). This contractive behavior, indicative of normal consolidation (Lambe and Whitman, 1969), is also exemplified by the stress path in Figure F8A, which moves to the upper left during shear. The stress-strain curve (Fig. F8B) levels off with strain rather than increasing, as it would if it were a highly dilatant sample. This behavior is quite different from the dilatational behavior of most dense sandy sediments tested in GHASTLI, whether the sediment contained gas hydrate or not (Winters et al., 2002). Contractive behavior induces a positive pore pressure response (reduces effective stress) and reduces shear strength, whereas dilatant behavior reduces pore pressure (increases effective stress) and increases strength (Fig. F8). For depositional environments in this region, the sediment is expected to weaken with shear because of the development of positive pore pressure.

### CONCLUSIONS

Preliminary acoustic, triaxial strength, and electrical resistivity results were presented from a test performed on a clayey silt sediment sample recovered from the summit of southern Hydrate Ridge during Leg 204. The test specimen was preserved in a methane-charged vessel and was the first sample to be airfreighted to a domestic destination in a DOT-exempted pressure vessel. The sample was tested using the Gas Hydrate and Sediment Test Laboratory Instrument (GHASTLI). Because little, if any, hydrate remained in the specimen during testing, we pre-

T2. Triaxial shear strength results, p. 19.

F8. Shear strength results, p. 17.



sented background physical property results for sediment that may host gas hydrate in situ. We consolidated the test specimen in increments beyond its in situ stress state to reduce the disturbance caused by the recovery process and to present properties representative of deeper sub-bottom sediment, assuming uniform stratigraphy.

$P$ -wave velocities from 1.54 to 1.74 km/s varied linearly with consolidation stress,  $\sigma'_c$ , up to 970 kPa. This trend reflects pure overburden effects without the influence of stratigraphic changes.  $V_p$  from adjacent well logs that are lower than those measured in GHASTLI for comparable subbottom depths may indicate the presence of free gas in situ.

Electrical resistivity was periodically measured by a Wenner array and varied from 1.0 to 2.8  $\Omega\text{m}$ . These values reflect both the pore water salinity and soft, fine-grained texture of the sediment. A trend of increasing electrical resistivity with consolidation stress is not seen in the well logs. This is probably due to the complex geologic structure of southern Hydrate Ridge, in combination with varying concentrations of pore water salinity and gas hydrates.

Shear behavior is consistent with the induced normally consolidated behavior of clayey silt. This type of behavior typically exhibits increasing pore pressure and a leveling off or decrease in strength during shear. This behavior is in marked contrast with other coarse-grained, hydrate-bearing samples we have tested in which the dilational nature of the sediment causes an increase in undrained strength with shear. Stability issues may therefore be more pronounced in the Hydrate Ridge region.

## **ACKNOWLEDGMENTS**

The authors wish to thank John Bratton, John Warner, Carolyn Ruppel, and an anonymous reviewer for their helpful comments and Dann Blackwood, Michelle Edwards, and Debbie Hutchinson for assistance during the setup procedure. Liz Beaulieu provided the grain-size information. We also wish to thank the Captain, crew, and scientists on board the *JOIDES Resolution* during Leg 204. This research used samples and/or data provided by the Ocean Drilling program (ODP). ODP is sponsored by the U.S. National Science Foundation (NSF) and participating countries under management of Joint Oceanographic Institutions (JOI), Inc. This work was supported by the Coastal and Marine Geology Program and Energy Program of the U.S. Geological Survey and partial funding was provided by the Gas Hydrate Program of the U.S. Department of Energy.

## REFERENCES

- ASTM International, 1997. Standard test method for specific gravity of solids by gas pycnometer (Standard D5550-94). In *Annual Book of ASTM Standards: Soil and Rock* (Vol. 04.09): West Conshohocken, PA (Am. Soc. Testing and Mater.), 380–383.
- Bohrmann, G., Greinert, J., Suess, E., and Torres, M., 1998. Authigenic carbonates from the Cascadia subduction zone and their relation to gas hydrate stability. *Geology*, 26:647–650. doi:10.1130/0091-7613(1998)026<0647:ACFTCS>2.3.CO;2
- Bowles, J.E., 1979. *Physical and Geotechnical Properties of Soils*: New York (McGraw-Hill).
- Holtz, R.D., and Kovacs, W.D., 1981. *An Introduction to Geotechnical Engineering*: Englewood Cliffs, NJ (Prentice-Hall).
- Hunt, R.E., 1984. *Geotechnical Engineering Investigation Manual*: New York (McGraw-Hill).
- Ladd, C.C., and Foott, R., 1974. A new design procedure for stability of soft clays. *J. Geotech. Div. (Am. Soc. Civ. Eng.)*, 100:763–786.
- Lambe, T.W., and Whitman, R.V., 1969. *Soil Mechanics*: New York (Wiley).
- Makogon, Y.F., 1997. *Hydrates of Hydrocarbons*: Tulsa (PennWell).
- Sharma, P.V., 1997. *Environmental and Engineering Geophysics*: Cambridge (Cambridge Univ. Press).
- Shipboard Scientific Party, 2003. Leg 204 summary. In Tréhu, A.M., Bohrmann, G., Rack, F.R., Torres, M.E., et al., *Proc. ODP, Init. Repts.*, 204: College Station TX (Ocean Drilling Program), 1–75. [HTML]
- Suess, E., Torres, M.E., Bohrmann, G., Collier, R.W., Greinert, J., Linke, P., Rehder, G., Tréhu, A., Wallmann, K., Winckler, G., and Zuleger, E., 1999. Gas hydrate destabilization: enhanced dewatering, benthic material turnover and large methane plumes at the Cascadia convergent margin. *Earth Planet. Sci. Lett.*, 170:1–15. doi:10.1016/S0012-821X(99)00092-8
- Tréhu, A.M., Long, P.E., Torres, M.E., Bohrmann, G., Rack, F.R., Collett, T.S., Goldberg, D.S., Milkov, A.V., Riedel, M., Schultheiss, P., Bangs, N.L., Barr, S.R., Borowski, W.S., Claypool, G.E., Delwiche, M.E., Dickens, G.R., Gracia, E., Guerin, G., Holland, M., Johnson, J.E., Lee, Y.-J., Liu, C.-S., Su, X., Teichert, B., Tomaru, H., Vanneste, M., Watanabe, M., and Weinberger, J.L., 2004. Three-dimensional distribution of gas hydrate beneath southern Hydrate Ridge: constraints from ODP Leg 204. *Earth Planet. Sci. Lett.*, 222:845–862. doi:10.1016/j.epsl.2004.03.035
- Tréhu, A.M., Torres, M.E., Moore, G.F., Suess, E., and Bohrmann, G., 1999. Temporal and spatial evolution of a gas hydrate-bearing accretionary ridge on the Oregon continental margin. *Geology*, 27(10):939-942. doi:10.1130/0091-7613(1999)027<0939:TASEOA>2.3.CO;2
- Winters, W.J., Dillon, W.P., Pecher, I.A., and Mason, D.H., 2000. GHASTLI: determining physical properties of sediment containing natural and laboratory-formed gas hydrate. In Max, M.D. (Ed.), *Coastal Systems and Continental Margins—Natural Gas Hydrate in Oceanic and Permafrost Environments*, (Vol. 5): Dordrecht, Netherlands (Kluwer), 311–322.
- Winters, W.J., Waite, W.F., Mason, D.H., Dillon, W.P., and Pecher, I.A., 2002. Sediment properties associated with gas hydrate formation. *Proc. 4th Int. Conf. Gas Hydrates*, 722–727.

Figure F1. Site location map for ODP Leg 204 (from Shipboard Scientific Party, 2003). NHR = northern Hydrate Ridge; SHR = southern Hydrate Ridge; SEK = Southeast Knoll. Smaller site designations represent original proposed identifiers.

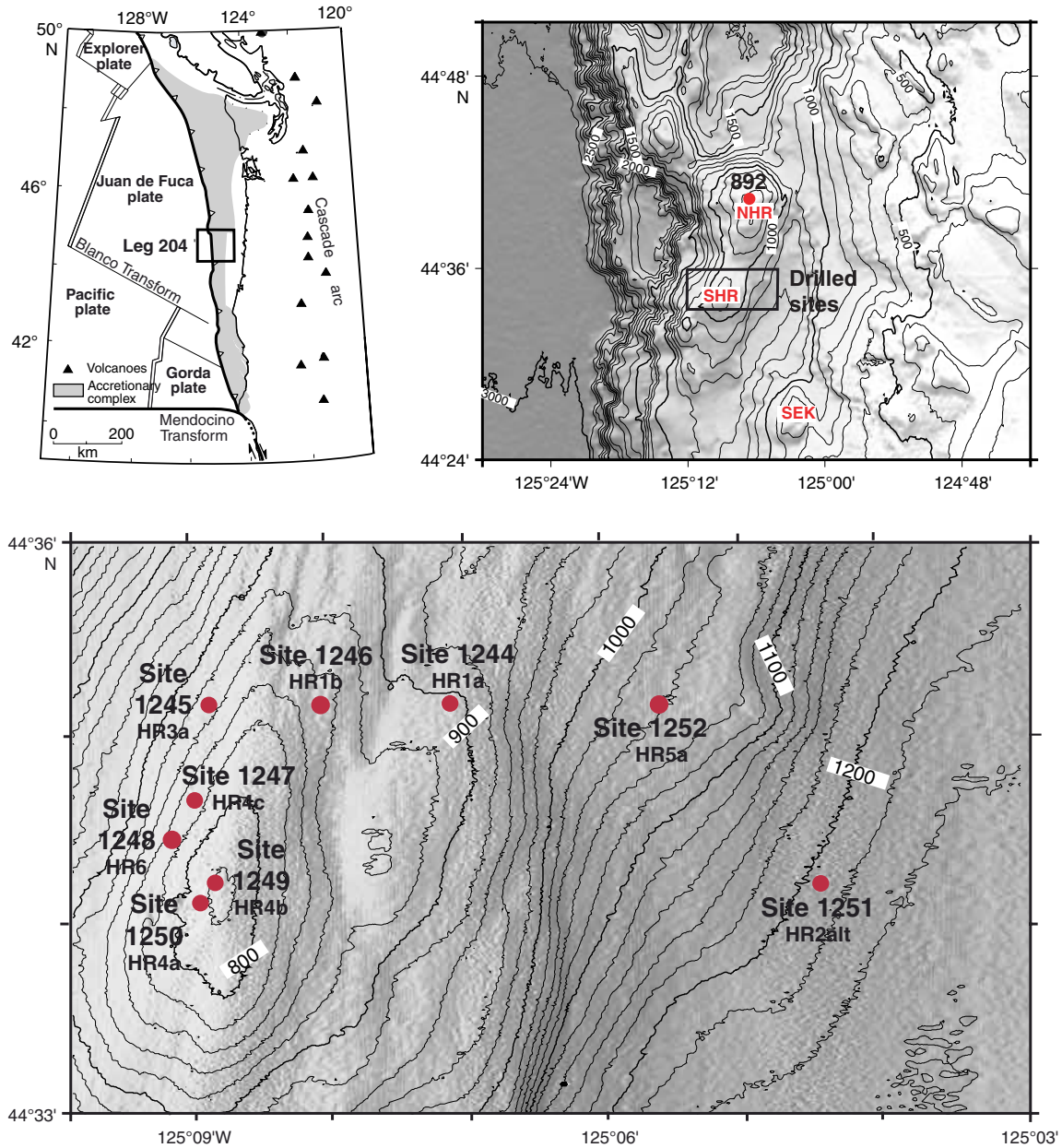
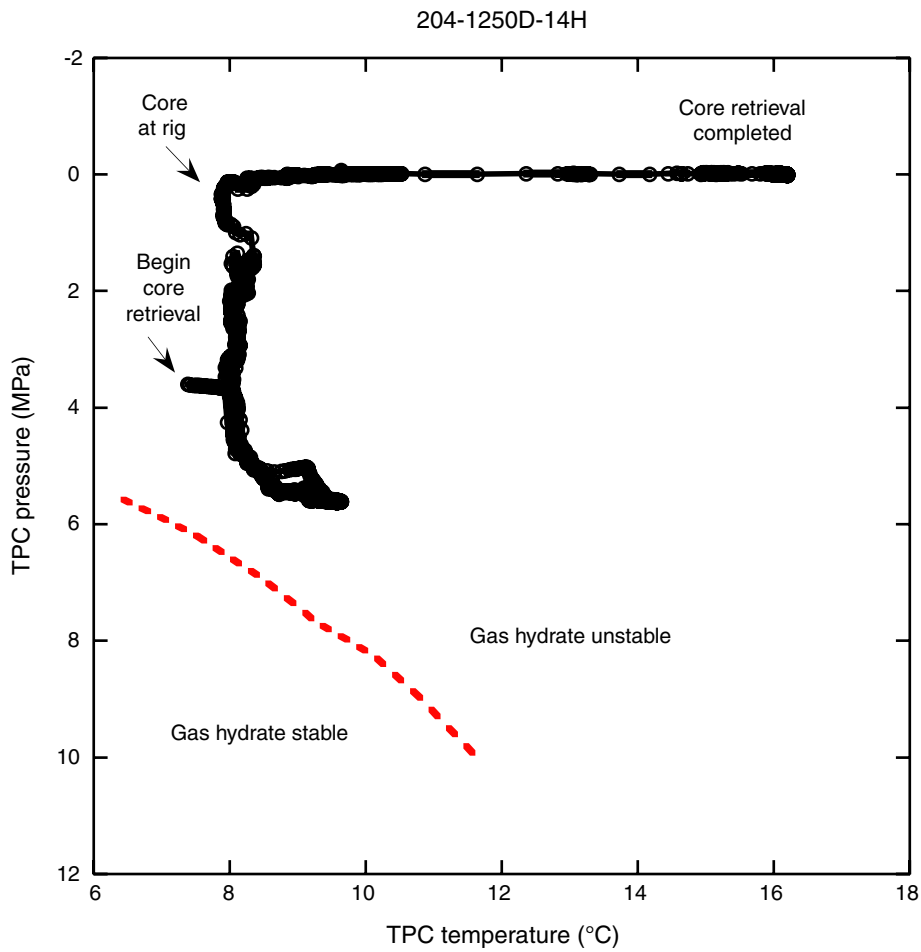


Figure F2. Pressure vs. temperature path for wireline retrieval of advanced piston coring (APC) Core 204-1250D-14H. Note that coring has caused the gas hydrate to leave the stability field even before the core has started its ascent. Data from [Ussler et al.](#), this volume. TPC = temperature, pressure, and conductivity measuring system in the APC piston head.



**Figure F3.** First domestic airfreight transportation of a DOT-exempted pressure vessel containing a methane hydrate test specimen. The cooler was packed with ice by ODP personnel in College Station, Texas, to keep potential gas hydrate below the dissociation temperature. The cooler was shipped from College Station to Woods Hole, Massachusetts.



**Figure F4.** Test sample after extrusion from the core liner, prior to end trimming and “dental” void-filling procedure. Note the friable nature of the very soft, clayey silt sediment.



**Figure F5.** Previous test specimen about to be raised into the main pressure vessel (visible at top of photograph). Test specimen (center of photograph) rests on an interchangeable internal load cell. A heat exchanger that imparts a unidirectional cooling front downward through the specimen rests atop the upper end cap, fed through the large diameter, vertical tubes at the front and rear of the specimen (Winters et al., 2000).

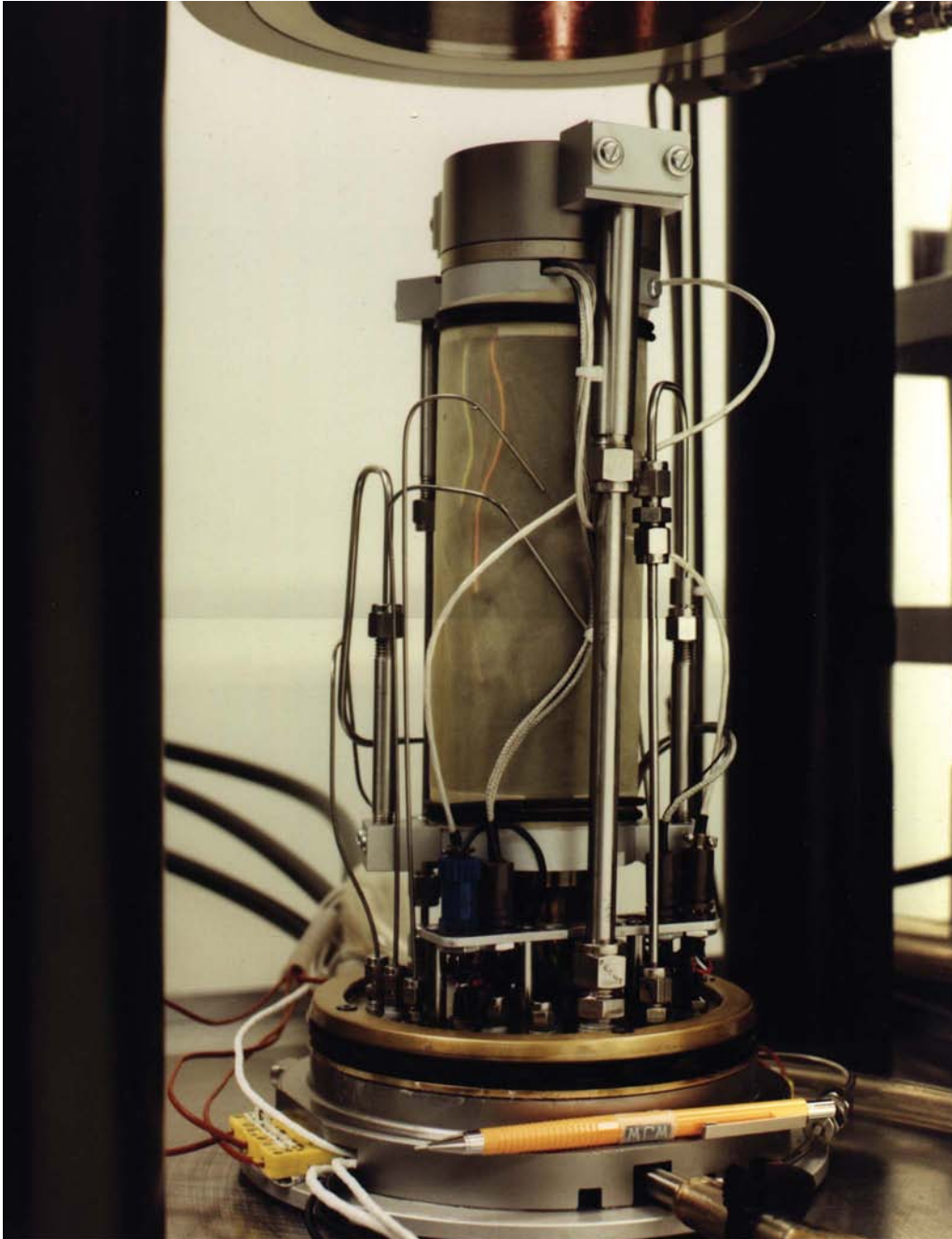


Figure F6. Measured  $P$ -wave velocity ( $V_p$ ) vs. consolidation stress ( $\sigma'_c$ ).

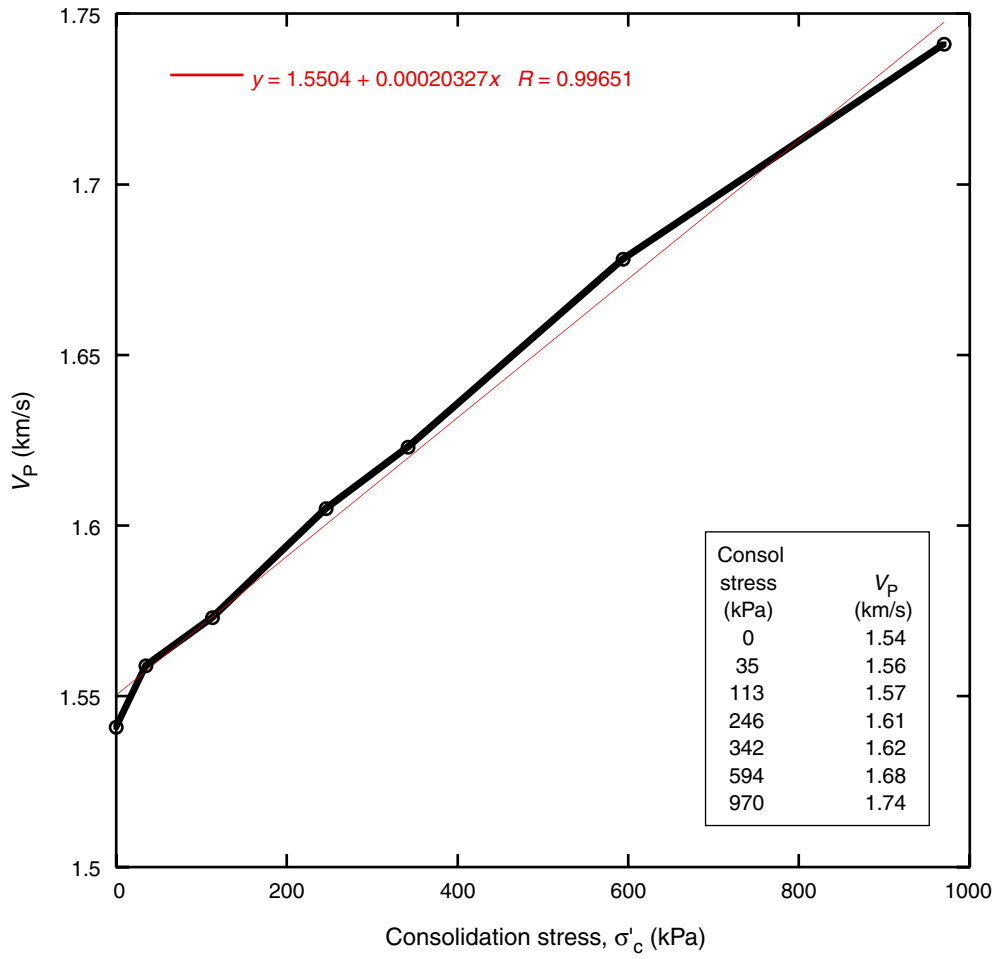
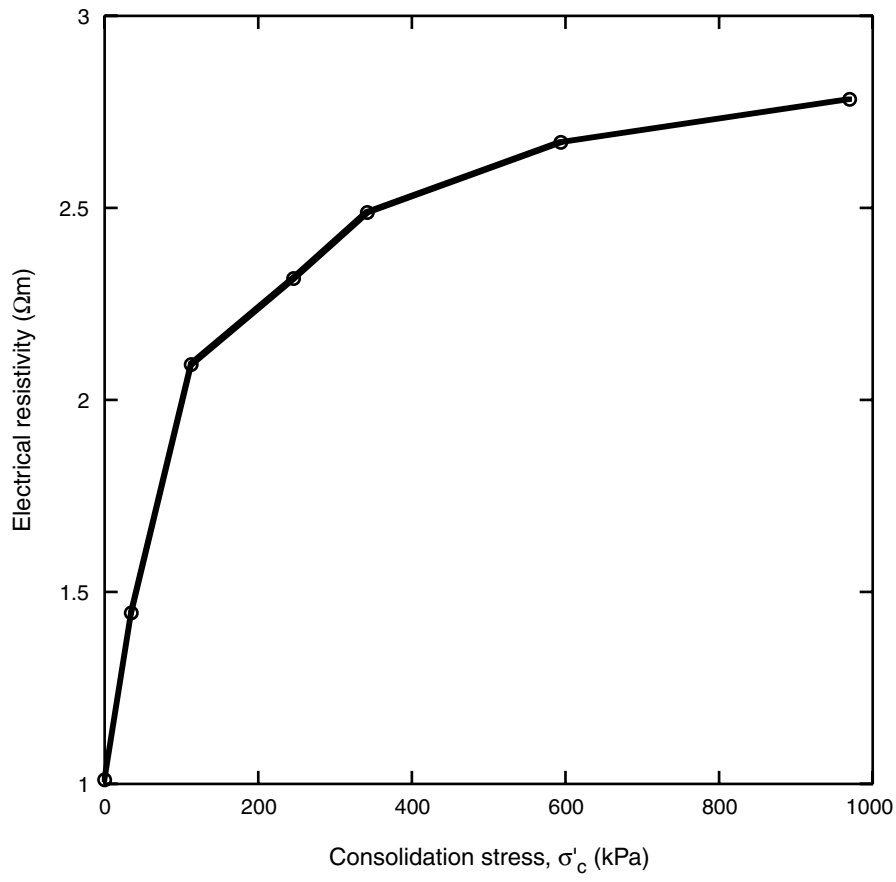
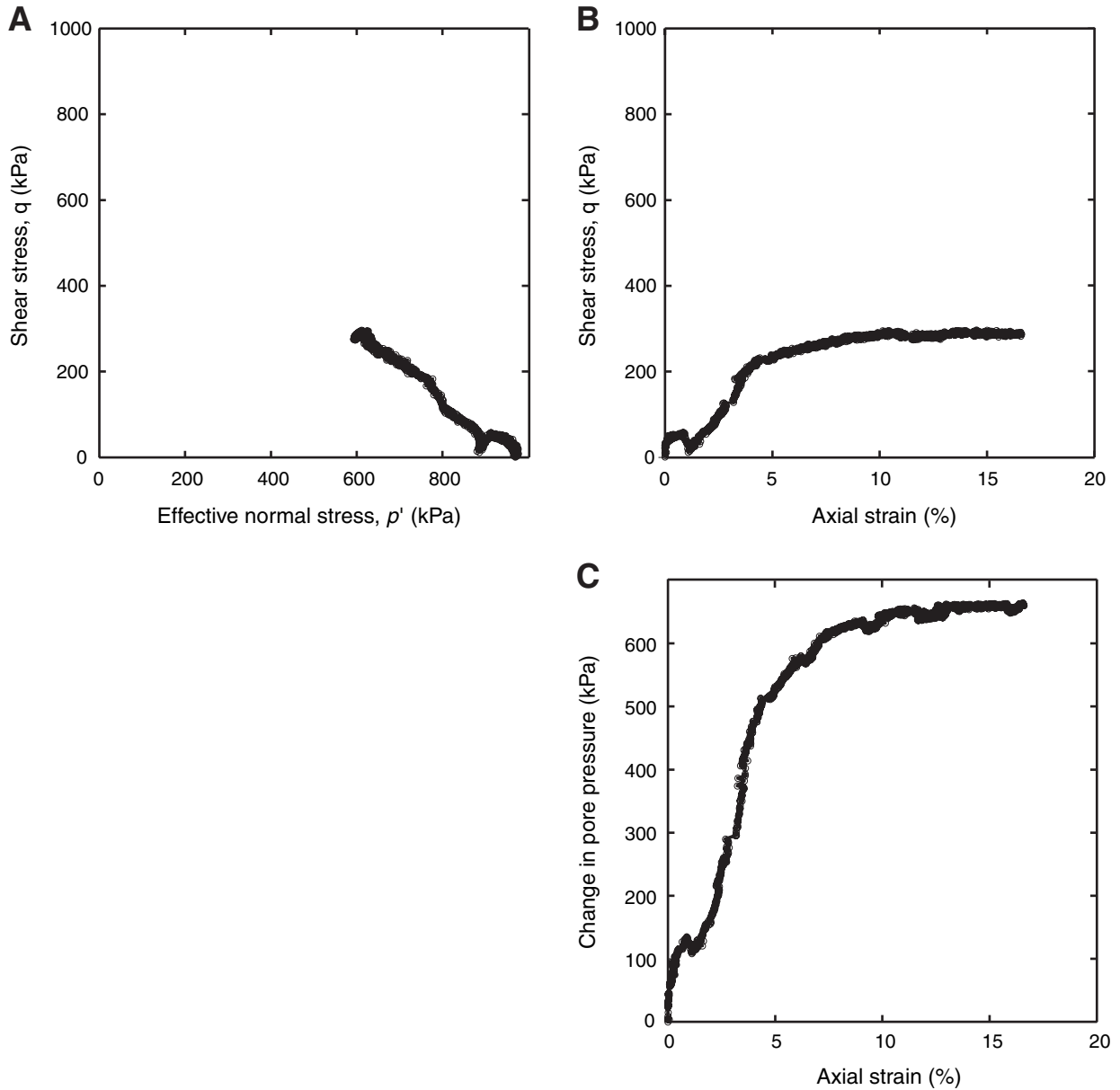


Figure F7. Electrical resistivity vs. consolidation stress ( $\sigma'_c$ ).



**Figure F8.** Shear strength results for test Sample GH101. **A.** Shear stress ( $q$ ) vs. effective normal stress ( $p'$ ) on a plane inclined at  $45^\circ$  from the horizontal. Each data point represents the top of a Mohr's circle and together they define a "stress path." **B.** Shear stress vs. axial strain. **C.** Change in pore pressure vs. axial strain. Note that electrical power was briefly interrupted at  $\sim 1\%$  strain, resulting in a decreased shear stress until power was restored. At the start of shear, plot A begins in the lower right corner on the horizontal axis and moves to the left, whereas plots B and C start in the lower left corner of the horizontal axis at  $0\%$  strain and move to the right.



**Table T1.** Moisture and density for the test specimen and trimmings.

GH101 summary	Test specimen		Trimmings		Final post shear
	Initial measured	Initial calculated	Initial 1	Initial 2	
Specimen volume (cm <sup>3</sup> )	381.4	367.7	41.0	23.5	328.9
Water content ( $M_w/M_s$ ) (%)		65.2	69.0	64.6	54.2
Water content ( $M_w/M_s$ ) (%)		39.5	40.8	39.2	35.2
Grain density (g/cm <sup>3</sup> )			2.67		
Bulk density (g/cm <sup>3</sup> )	1.58	1.64	1.61	1.64	1.71
Unit weight (kN/m <sup>3</sup> )	15.47	16.05	15.84	16.09	16.76
Void ratio	1.79	1.69	1.79	1.68	1.41
Porosity (%)	64.2	62.9	64.2	62.7	58.5
Void saturation by water (%)	94.4	100.0	100.0	100.0	100.0
Grain size					
Sand (%)				0.8	
Silt (%)				56.5	
Clay (%)				42.7	
Mean ( $\phi$ )				7.75	

Note: "Calculated" values assume 100% of the pore space was saturated with water.

**Table T2.** Triaxial shear strength results.

Test	Result
Consolidation stress, $\sigma'_c$ (kPa)	970
"A" coefficient at failure	1.12
$q$ at failure ( $q_{max}$ ) (kPa)	297
$p'$ at failure (kPa)	612
$q_{max}/\sigma'_c$	0.31
Deviator stress at failure (kPa)	594
Axial strain at failure (%)	14.5
$\phi'_{max}$ (degrees)	29.0

Notes: Consolidation stress = difference between confining and internal pore pressure prior to shear. "A" coefficient at failure = change in pore pressure/change in deviator stress,  $q$  = shear stress acting on a plane inclined  $45^\circ$  from the horizontal,  $(\sigma_1 - \sigma_3)/2$ ,  $p'$  = normal effective stress acting on a plane inclined  $45^\circ$  from the horizontal,  $(\sigma_1 + \sigma_3)/2$ ,  $\phi'_{max}$  = maximum friction angle in terms of effective stresses, passes through the origin.